JACS
JOURNAL OF THE AMERICAN CHEMICAL SOCIETY
Article
pubs.acs.org/JACS

# Chiral Metallohelical Complexes Enantioselectively Target Amyloid β for Treating Alzheimer's Disease

Meng Li,[†] Suzanne E. Howson,[‡] Kai Dong,[†] Nan Gao,[†] Jinsong Ren,[†] Peter Scott,[‡] and Xiaogang Qu*[,†]

[†]Laboratory of Chemical Biology, Division of Biological Inorganic Chemistry, State Key Laboratory of Rare Earth Resource Utilization, Changchun Institute of Applied Chemistry, University of Chinese Academy of Sciences, Chinese Academy of Sciences, Changchun, Jilin 130022, China

[‡]Department of Chemistry, University of Warwick, Gibbet Hill Road, Coventry CV4 7AL, United Kingdom

Supporting Information

**ABSTRACT:** Stereochemistry is a very important issue for the pharmaceutical industry and can determine drug efficacy. The design and synthesis of small molecules, especially chiral molecules, which selectively target and inhibit amyloid-β (Aβ) aggregation, represent valid therapeutic strategies for treatment of Alzheimer's disease (AD). Herein we report that two triple-helical dinuclear metallosupramolecular complexes can act as a novel class of chiral amyloid-β inhibitors. Through targeting α/β-discordant stretches at the early steps of aggregation, these metal complexes can enantioselectively inhibit Aβ aggregation, which is demonstrated using fluorescent living cell-based screening and multiple biophysical and biochemical approaches. To the best of our knowledge, this is the first report of enantioselective inhibition of Aβ aggregation. Intriguingly, as a promising candidate for AD treatment, the chiral metal complex can cross the blood−brain barrier and have superoxide dismutase activity. It is well-known that chiral discrimination is important for understanding chiral drug action. Generally, one enantiomer is pharmaceutically active while the other is inactive or exerts severe side effects. Chiral discrimination should be important for AD treatment. Our work provides new insights into chiral inhibition of Aβ aggregation and opens a new avenue for design and screening of chiral agents as Aβ inhibitors against AD.

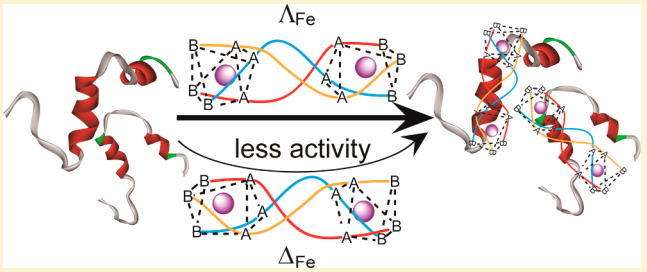


## INTRODUCTION

Alzheimer's disease (AD) is the most common form of dementia, which afflicts more than 24 million people worldwide.[1,2] A significant body of data has indicated that polymerization of amyloid-β (Aβ) peptide into amyloid fibrils is a critical step in the pathogenesis of AD.[3−7] Therefore, inhibition of Aβ aggregation has been considered as an attractive therapeutic and preventive strategy for AD treatment. Although considerable progress has been achieved in discovering inhibitors of Aβ aggregation and toxicity,[8−10] chiral recognition of Aβ and aggregation morphology can provide more information on Aβ effects involved in AD pathogenesis, and there are no reports of enantioselective targeting and inhibition of Aβ aggregation.[11] As indicated previously, it is extremely important to explore drug enantioselectivity because usually just one of the enantiomers is pharmaceutically active while the other is inactive or exerts severe side effects.[12,13] Therefore, chiral recognition may be a crucial subject for treatment of AD.

It has been demonstrated that Aβ harbors an α-helix in the 13−23 segment, although this segment should be predicted to form a β-strand.[14] Owing to the critical role of α/β discordance in Aβ fibril formation, we and others[15,16] recently indicated that targeting the α-helical form of this region in Aβ peptide could be a novel approach for designing and screening inhibitors of Aβ aggregation. Because of the chirality of the α-helical structure and the L-amino acids that comprise the peptides, Aβ is sensitive to a chiral environment and the interaction between Aβ and the chiral inhibitor exhibits a specific orientation.[17] Chiral supramolecular complexes which are suitable for binding and targeting the α-helical form of the 16−23 region may show an enantioselective effect on inhibiting Aβ fibrillation.

Herein, to achieve chiral recognition of Aβ, we strategically prepared thermodynamically stable single enantiomers of monometallic units[18−20] connected by organic linkers, $[Fe_2L^1_3]Cl_4$ ($\Lambda_{Fe}$,$S_C$-$[Fe_2L^1_3]Cl_4$ and $\Delta_{Fe}$,$R_C$-$[Fe_2L^1_3]Cl_4$) and $[Fe_2L^2_3]Cl_4$ ($\Lambda_{Fe}$,$R_C$-$[Fe_2L^2_3]Cl_4$ and $\Delta_{Fe}$,$S_C$-$[Fe_2L^2_3]Cl_4$), to enantioselectively target and inhibit Aβ aggregation. This highly adaptable self-assembly approach enables rapid preparation of ranges of water-stable, helicate-like compounds with high stereochemical purity. Both $[Fe_2L^1_3]Cl_4$ (complex **1**) and $[Fe_2L^2_3]Cl_4$ (complex **2**) commonly comprise a chiral assembly of three ditopic bidentate organic ligands around two metal centers (Figure S1, Supporting Information). With a diameter of ∼1.2 nm (similar to that of a typical α-helix peptide), these metal complexes can be promising candidates for enantioselective inhibition of Aβ fibrillation (Scheme 1). To the best of

**Received:** March 19, 2014
**Published:** July 25, 2014

   dx.doi.org/10.1021/ja502789e | J. Am. Chem. Soc. 2014, 136, 11655−11663

our knowledge, this is the first example to show that one of the enantiomers can selectively target and inhibit A$\beta$ aggregation.

**Scheme 1. Representative Illustration of Chiral Metallosupramolecular Complexes Enantioselectively Bound to A$\beta$**

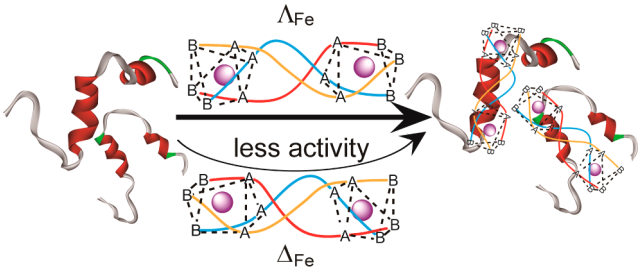


## METHODS

**Construction of the A$\beta$−ECFP (Enhanced Cyan Fluorescent Protein) Fusion System.** The A$\beta$−ECFP fusion system we constructed was similar to that previously reported by Hecht and co-workers.[21,22] The A$\beta$1−42 and ECFP coding sequences were incorporated together by a short linker DNA. *Escherichia coli* strain BL21 (DE3) was transformed by the vector (A$\beta$−linker−ECFP) or the control vector (linker−ECFP) and cultured at 37 °C in LB (lysogeny broth) medium containing 50 $\mu$g mL$^{-1}$ ampicillin. Metallosupramolecular complexes with different concentrations were added to the culture 30 min prior to protein expression induced by 1 mM isopropyl $\beta$-D-thiogalactoside (IPTG). After the expression of the recombinant proteins for 3 h, all the samples were diluted to 0.1 OD (optical density) at 600 nm. Fluorescence measurements were carried out by using a JASCO-FP6500 spectrofluorimeter. The excitation wavelength was 433 nm.

**Peptide Preparation.** A$\beta$25−35 (lot no. 70K49532) and A$\beta$12−28 (lot no. 32K12201) were purchased from Sigma, and A$\beta$1−40 (lot no. U10012) was obtained from American Peptide. The peptides were prepared as described previously.[16,21] Briefly, the peptide was dissolved in HFIP at a concentration of 1 mg mL$^{-1}$ with shaking at 4 °C for 4 h in a sealed vial for further dissolution. It was then stored at −20 °C as a stock solution. Before the experiments, the solvent HFIP was removed by evaporation under a gentle stream of nitrogen and the peptide was dissolved in aggregation buffer (10 mM HEPES, 150 mM NaCl, pH 7.3). For the preparation of fibrils (fA$\beta$), A$\beta$1−40 or A$\beta$25−35 solutions were incubated at 37 °C for 7 days.

**Thioflavin T (ThT) Binding Fluorescence.** At different times, all A$\beta$1−40 aliquots in the absence or presence of metal complexes were diluted 80-fold in preparation for the ThT binding assay using a JASCO-FP6500 spectrofluorimeter. The final concentration of ThT was 10 $\mu$M. The excitation wavelength was 444 nm, and the emission intensity at 482 nm was used for analysis.

**Atomic Force Microscopy (AFM) Imaging.** A 50 $\mu$M concentration of A$\beta$1−40 and 50 $\mu$M A$\beta$1−40 in the presence of equimolar complex **1** or complex **2** were incubated for 7 days at 37 °C. Samples were prepared as described previously.[16] Briefly, the samples were diluted with deionized $H_2O$ to yield a final concentration of 1 $\mu$M. Then aliquots of 50 $\mu$L of each sample were placed on a freshly cleaved mica substrate. After incubation for 5 min, the substrate was rinsed twice with water and dried before measurement. Tapping mode was used to acquire the images under ambient conditions.

**Circular Dichroism (CD) Measurements.** CD spectra were collected at 37 °C with a JASCO J-810 spectropolarimeter using a 1 mm path length quartz cell. The parameters were controlled as 0.1 nm intervals and 4 s response, and the spectrum of each sample was an average of three scans at a speed of 5 nm min$^{-1}$ over the wavelength range from 200 to 250 nm.

**Sedimentation and Electrophoresis Assay.** A$\beta$1−40 peptide (50 $\mu$M) in the absence or presence of 50 $\mu$M metal complexes was incubated at 37 °C for 7 days. The aggregated peptide in each sample was separated by centrifugation at 13 500 rpm for 20 min at 20 °C. The pellets were resuspended and boiled after the addition of sample buffer. Samples were run on a 12% Tris−Tricine sodium dodecyl sulfate (SDS) gel at 100 V for 1 h, followed by silver staining.

**Trypsin Digestion.** A$\beta$12−28 (10 $\mu$L, 20 $\mu$M) was incubated at 37 °C for 1 h with trypsin (0.1 mg mL$^{-1}$) in the absence or presence of increasing concentrations of complex **2**. At the end of the reaction, all samples were supplemented with SDS−PAGE reducing sample buffer, and heated at 100 °C for 5 min. Gels were run in a Tris−Tricine system, after which the gels were silver-stained. Lysozyme, which can also be digested by trypsin, was used as the control.

**NMR Spectroscopy.** Samples for NMR were run in aqueous Tris buffer (10 mM Tris, 150 mM NaCl, pH 7.3) with 10% $D_2O$ added. Samples containing A$\beta$1−40 were run at 0.1 mM. The metal complexes $\Lambda_{Fe}$,$R_C$-[$Fe_2L^2_3$]$Cl_4$ and $\Delta_{Fe}$,$S_C$-[$Fe_2L^2_3$]$Cl_4$ were incubated with A$\beta$1−40 at 37 °C for 2 h. NMR measurements were carried out on a Bruker 600 MHz AVANCE NMR spectrometer equipped with a triple-channel cryoprobe at 5 °C. The concentrations of the metal complexes were 0.1 mM.

**Docking Studies.** The structure of the A$\beta$1−40 (aqueous solution NMR structure, PDB 2LFM) was obtained from the Protein Data Bank. Specifically, the structures of A$\beta$1−40 and the four metal complexes (complexes **1** and **2**) were prepared in the standard manner using AutoDock Tools. All torsion angles for each compound were considered flexible. Using AutoDock Vina, binding calculations were made between A$\beta$1−40 and the metal complexes. In this study, a grid of 126 Å × 126 Å × 126 Å was constructed with a spacing of 0.375 points/Å to cover the entire molecule. The center of the grids was placed at the center of mass of A$\beta$1−40. For reliable calculations, the exhaustiveness for the docking runs was set at 400 and the other parameters were kept as default values. During docking, 20 binding modes (20 modes of docking) were generated with random starting positions of the metal complexes. Docked models of the metal complexes were visualized with A$\beta$1−40 using Discovery Studio.

**Reactive Oxygen Species (ROS) Detection.** PC12 cell (rat pheochromocytoma, American Type Culture Collection) cultures grown on 24-well plates were incubated with 50 $\mu$M 2′,7′-dichlorofluorescin (DCF) diacetate (Beyotime, China) for 30 min at 37 °C after 12 h with the samples. The cells were then rinsed with PBS solution. Intracellular esterases convert DCF diacetate to anionic DCFH, which is trapped in the cells. The fluorescence of DCF, formed by the reaction of DCFH with ROS, was examined with a spectrofluorometer (JASCO-FP6500, Japan).

**Superoxide Dismutase (SOD) Activity Determination.** The SOD activities of these metal complexes were assayed by measuring inhibition of the photoreduction of nitro blue tetrazolium (NBT). The solutions containing riboflavin (20 $\mu$M), methionine (0.013 M), NBT (75 $\mu$M), and metal complexes of various concentrations were prepared with 50 mM phosphate buffer (pH 7.8). The mixtures were illuminated by a lamp with a constant light intensity for 10 min at 25 °C. After illumination, immediately the absorbance was measured at 560 nm. The entire reaction assembly was enclosed in a box lined with aluminum foil. Identical tubes with the reaction mixture were kept in the dark and served as blanks. The inhibition percentage was calculated according to the following formula: inhibition (%) = $[(A_0 - A)/A_0] \times 100$, where $A_0$ is the absorbance of the control and $A$ is the absorbance of the sample.

**Cell Culture and Neurotoxicity Assay.** PC12 cells (rat pheochromocytoma, American Type Culture Collection) were maintained in Iscove's modified Dulbecco's medium (IMDM) (Gibco, BRL) supplemented with 5% fetal bovine serum and 10% heat-inactivated horse serum at 37 °C in a humidified atmosphere of 5% $CO_2$ and 95% air. Differentiation was induced by 50 $\mu$g mL$^{-1}$ nerve growth factor (NGF) (Invitrogen) until about 80% cells extended neuronal-like processes. The cells were plated at 30 000 cells per well on poly-L-lysine-coated 96-well plates in fresh medium. After 24 h, A$\beta$1−40 peptides (5 $\mu$M) that had been aged with or without various concentrations of metal complexes were dispensed into the PC 12 cells, and the cells were further incubated for 36 h at 37 °C.


dx.doi.org/10.1021/ja502789e | J. Am. Chem. Soc. 2014, 136, 11655−11663

Cytotoxicity was measured by using a modified MTT (3-(4,5-dimethylthiazol-2-yl)-2,5-diphenyltetrazolium bromide) assay kit (Promega). Absorbance values of formazan were determined at 490 nm with an automatic plate reader. All tests were repeated three times in quadruplicate wells.

**Assay of Intracellular Free Calcium.** PC12 cells were plated at a density of $3 \times 10^5$ cell/mL on glass coverslips coated with poly-L-lysine. Two days later, the cells, when at approximately 80% confluence, were exposed to either A$\beta$ or A$\beta$ plus the metal complexes for 2 h. The cells were then washed and fixed with paraformaldehyde (4%) for 10 min at room temperatures. The fixed cells were incubated at 37 °C for 1 h in IMDM serum-free medium containing 3 $\mu$M Fluo-3 AM (Beyotime, China). Fluorescence from Fluo-3 AM was captured using flow cytometry. The excitation wavelength was 488 nm.

## RESULTS AND DISCUSSION

By using a high-throughput screening method based on the fluorescence of an A$\beta$−ECFP fusion expression system constructed in our laboratory[16,21,23] which was originally developed by Hecht and co-workers,[22] we have identified the two pairs of metal complexes capable of inhibiting A$\beta$ aggregation (Figure 1A). ECFP folds into its native state

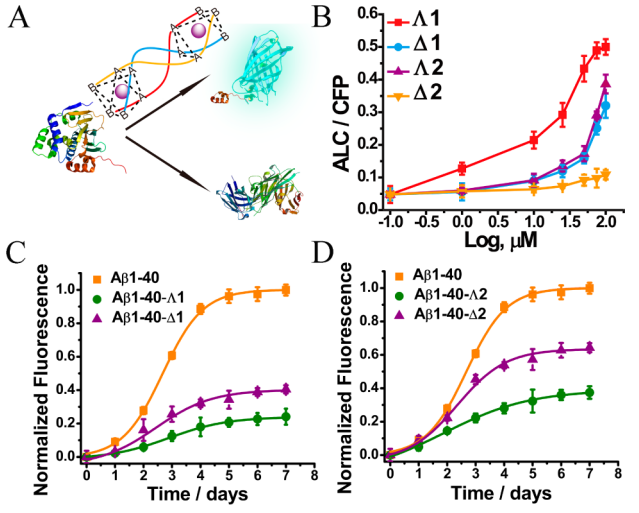


**Figure 1.** (A) Schematic representation of screening A$\beta$ aggregation inhibitors using the A$\beta$−linker−ECFP fusion screen system. (B) Screening results from the screen system. The inhibition effect of metal complexes showed both structural and chiral selectivity. Fibrillation kinetics of A$\beta$1−40 as monitored by the development of thioflavin T binding in the absence or presence of (C) complex **1** and (D) complex **2**. The A$\beta$1−40 concentration was 50 $\mu$M, and the metal complex concentrations were 10 $\mu$M. The samples were measured in 10 mM HEPES (pH 7.3) after incubation at 37 °C for 7 days.

slowly, and the fluorescence of the A$\beta$−ECFP fusion depends on A$\beta$ folding and solubility. A$\beta$ aggregation can lead to the entire A$\beta$−ECFP fusion misfolding and not emitting fluorescence. Inhibitors that can block or retard A$\beta$ aggregation would enable ECFP to fold into its native structure to recover its fluorescence. Figure 1B unambiguously indicates that all of these metal complexes could strongly inhibit A$\beta$ aggregation. In the presence of these metal complexes, metal complex concentration-dependent fluorescence enhancement was observed. Complex **1** had significantly higher inhibition activity compared to complex **2**. Further study demonstrated that enantiomers **Λ1** ($\Lambda_{Fe}$,$S_C$-$[Fe_2L^1{}_3]Cl_4$) and **Λ2** ($\Lambda_{Fe}$,$R_C$-$[Fe_2L^2{}_3]Cl_4$) exhibited higher inhibition effects on A$\beta$ aggregation than their mirror images **Δ1** ($\Delta_{Fe}$,$R_C$-$[Fe_2L^1{}_3]Cl_4$) and **Δ2** ($\Delta_{Fe}$,$S_C$-$[Fe_2L^1{}_3]Cl_4$), respectively. Importantly, the enantioselectivity of complex **2** was even more obvious than that of complex **1**. Control experiments showed that almost no fluorescence enhancements were observed for the non-A$\beta$ fusion system (Figure S2, Supporting Information), indicating that the fluorescence enhancements were not due to the interactions of these complexes with the fluorescent protein.

To verify the effect of the absolute configuration of the metal complex on the assembly of A$\beta$1−40 into amyloid fibrils, we employed the commonly used ThT fluorescence assay (Figure 1C,D). ThT, an extrinsic fluorescent dye, is able to bind to amyloid fibrils; upon binding, its fluorescence intensity increases.[24−26] When fresh A$\beta$1−40 alone was incubated at 37 °C, ThT fluorescence showed a sigmoidal shape as a function of the incubation time (Figure 1C). This result was consistent with the nucleation-dependent polymerization model. However, all these metal complexes can decrease ThT fluorescence in a dose-dependent manner (Figure S3, Supporting Information). $IC_{50}$ values were estimated to be 1.69 $\mu$M for **Λ1**, 5.43 $\mu$M for **Δ1**, 6.62 $\mu$M for **Λ2**, and 42.2 $\mu$M for **Δ2** (Table 1). In control experiments, metal complex alone

**Table 1. $IC_{50}$ Values ($\mu$M) of Complexes 1 and 2 for Inhibition of Fibril Formation and Destabilization of the Preformed Fibrils**

| | inhibition | | destabilization | |
|---|---|---|---|---|
| metal complex | A$\beta$1−40 | A$\beta$25−35 | A$\beta$1−40 | A$\beta$25−35 |
| **Λ1** | 1.69 ± 0.23 | 36.38 ± 4.59 | 1.97 ± 0.46 | 41.19 ± 2.94 |
| **Δ1** | 5.43 ± 0.86 | >50 | 8.53 ± 0.71 | >50 |
| **Λ2** | 6.62 ± 0.58 | >50 | 9.82 ± 1.23 | >50 |
| **Δ2** | 42.21 ± 6.13 | >50 | >50 | >50 |

did not influence ThT fluorescence under our experimental conditions (Figure S4, Supporting Information). These preliminary $IC_{50}$ data indicated two trends in the antiaggregation activity of the flexicates. First, systems with less polar ligands (complex **1**) were more effective. Second, the $\Lambda_{Fe}$ enantiomers showed more effective activities than the $\Delta_{Fe}$ enantiomers. Furthermore, the decreased ThT fluorescence almost reached a maximum at an equal concentration of metal complex (Figure S3). This is consistent with A$\beta$1−40 interacting with the metal complex in a 1:1 ratio, as has been observed previously.[27] This suggests that binding occurred in the early stages of the aggregation process,[24−26] whereby the metal complex inhibits oligomerization of A$\beta$ monomers to inhibit the formation of the early soluble A$\beta$ oligomers. Such soluble aggregates are reported to make a greater contribution to neurotoxicity in AD than the insoluble extracellular A$\beta$ deposits.[28,29]

The inhibition of A$\beta$ aggregation was further investigated via an SDS−PAGE assay.[30,31] After incubation for 7 days, the large molecular weight A$\beta$1−40 aggregates were separated from the low molecular weight A$\beta$ species by spinning down the samples. The aggregated peptide pellets were resuspended and boiled after addition of sample buffer and were run on the SDS−PAGE assay to check the total amounts of aggregated A$\beta$. Our results showed that after incubation with complexes **1** and **2**, the quantity of the resuspended peptide was significantly decreased, especially for **Λ1** (Figure S5, Supporting Information), indicating that these metal complexes inhibit A$\beta$ aggregation.


dx.doi.org/10.1021/ja502789e | J. Am. Chem. Soc. 2014, 136, 11655−11663

We also investigated the effect of these metal complexes on the morphology of A$\beta$1−40 aggregates using AFM.[32−34] As shown in Figure 2A, classical amyloid fibrils were observed in

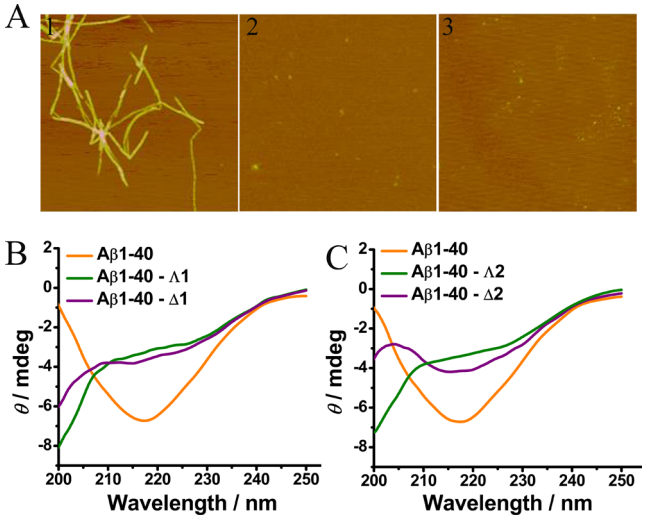


**Figure 2.** (A) The morphology of A$\beta$1−40 aggregates was analyzed by AFM images (area corresponding to 2.5 $\mu$m × 2.5 $\mu$m): (1) 50 $\mu$M A$\beta$1−40, (2) 50 $\mu$M A$\beta$1−40 in the presence of 50 $\mu$M complex **Λ1**, (3) 50 $\mu$M A$\beta$1−40 in the presence of 50 $\mu$M complex **Δ1**. The ability of (B) complex **1** and (C) complex **2** to inhibit A$\beta$1−40 aggregation was monitored by CD assay. The A$\beta$1−40 concentration was 50 $\mu$M, and the metal complex concentrations were 10 $\mu$M. The samples were measured in 10 mM HEPES (pH 7.3) after incubation at 37 °C for 7 days.

samples of untreated A$\beta$1−40. The A$\beta$1−40 fibrils were nonbranched, helical filaments with diameters of ∼10 nm and lengths of up to several micrometers. When A$\beta$1−40 was incubated with the metal complexes, especially with **Λ1**, numerous small, relatively amorphous aggregates were observed, demonstrating the excellent efficacy of metal complexes to inhibit A$\beta$1−40 aggregation (Figure 2A; Figure S6, Supporting Information). A$\beta$ oligomers, protofibrils, and fibrils all share the common $\beta$-sheet structure which drives A$\beta$ aggregation and toxicity. Circular dichroism studies (Figure 2B,C) indicated that all these metal complexes could inhibit structural transition from the native A$\beta$1−40 random coil to the $\beta$-sheet conformation in solution. Our inhibition data further demonstrated that these two metallosupramolecular complexes could inhibit A$\beta$ self-assembly at the early steps, in agreement with the cell-based screening results and ThT fluorescence and AFM data.

Intriguingly, free ligand L (*R* or *S*) showed little inhibition effect and chiral discrimination on A$\beta$ aggregation (Figure S7, Supporting Information). When assembled into a triple-helicate metallosupramolecular structure, these metal complexes could not only inhibit A$\beta$ aggregation but also destabilize preformed fibrils (Figure S8, Supporting Information; Table 1) with enantioselectivity. Furthermore, upon A$\beta$1−40 binding, the spectral position and intensity of the metal-to-ligand charge-transfer (MLCT) bands of the metallosupramolecular complex did not change (Figure S9, Supporting Information), indicating that A$\beta$ binding did not destroy the metal complex rigid structure.[18−20]

To further support the enantioselective nature of inhibition, dialysis experiments[35−38] were designed to reveal the structural selectivity of these metal complex enantiomers. Racemic mixtures of complex **1** or **2** were prepared by mixing equimolar amounts of the pure enantiomers (Figure 3A,B). The mixture

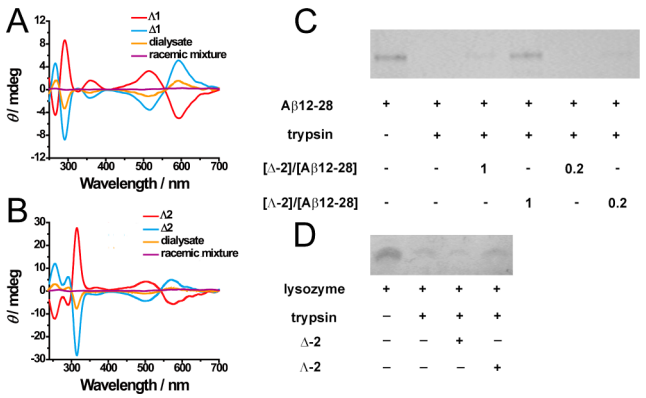


**Figure 3.** CD spectra of the dialysate for enrichment in the enantiomer with poorer affinity for the A$\beta$1−40 contained within the dialysis tube in a competition dialysis experiment: (A) complex **1**, (B) complex **2**. SDS−PAGE analysis of the effect of complex **2** on tryptic digests of (C) A$\beta$12−28 and (D) lysozyme was used as the control. Experimental details are described in the Methods.

was dialyzed against A$\beta$1−40, and circular dichroism was used to monitor the dialysate for enrichment of the enantiomer with lower binding affinity to A$\beta$1−40 in the dialysis tube. As shown in Figure 3A,B, the dialysate was enriched in **Δ1** and **Δ2**, respectively. These results indicated unambiguously that **Λ1** and **Λ2** bound preferentially to A$\beta$1−40 compared with their mirror images.

ESI-MS[28,29] was also employed to compare the binding ability of the metal complexes to A$\beta$. Here we took complex **2** as an example since the chiral discrimination between the two enantiomers was more obvious. As shown in Figure S10A (Supporting Information), the A$\beta$1−40 peptide alone gave two peaks at 1083 and 1444, corresponding to the 4+ and 3+ ionization states of the A$\beta$1−40 monomer, respectively. However, after treatment of A$\beta$1−40 with complex **2**, extra peaks were observed at 1208 and 1509 in the mass spectrum (Figure S10C,D), which corresponded to the 1:1 metal complex−A$\beta$ monomer complex. These results further supported that the metal complexes bound to A$\beta$ peptide in a 1:1 binding ratio. Intriguingly, after treatment of the A$\beta$ peptide with **Λ2**, the metal complex fragment peaks in the mass spectrum were weaker than those for the samples treated with **Δ2**, indicating that A$\beta$1−40 bound more tightly to **Λ2** to prevent the metal complex from being ionized, which would be supported by our next quantitative fluorescence titration studies.

The four metal complexes showed different inhibition abilities. To gain better understanding of the inhibition effects of the metal complexes, we compared the binding affinities of the four metal complexes to A$\beta$1−40 by using the fluorescence titration method.[39,40] The fluorescence intensity of A$\beta$1−40 was quenched with increasing amounts of metal complexes. The apparent binding constants (Table 2) obtained by a nonlinear least-squares fit which had been corrected for the inner filter effect[41,42] (Figure S11, Supporting Information; Table 2) were in agreement with the $IC_{50}$ values of the metal complexes against A$\beta$1−40 aggregation (Table 1). Therefore, we concluded that the different inhibition abilities of these


dx.doi.org/10.1021/ja502789e | J. Am. Chem. Soc. 2014, 136, 11655−11663

**Table 2. Binding Constants of Different Metal Complexes with Aβ1−40**

| | Λ1 | Δ1 | Λ2 | Δ2 |
|---|---|---|---|---|
| binding constant[a] ($M^{-1}$) | $3.81 \times 10^6$ | $9.62 \times 10^5$ | $1.04 \times 10^6$ | $1.97 \times 10^5$ |

[a]The binding constant was measured by the fluorescence titration method and obtained by a nonlinear least-squares fit which corrected for the inner filter effect. The values are the average of two independent measurements. The experimental details are described in the Supporting Information.

given metal complexes depended mainly on the different binding affinities to Aβ1−40. Although complexes **1** and **2** had similar triple-helical structures, the two iron helices showed different Aβ inhibition activities and binding affinities due to their different ligands. The more flexibly linked complex **2** had a weaker hydrophobic interaction and π−π stacking with the peptide. Noteworthy, although the binding affinities of metal complexes to Aβ1−40 were not as high as those to Aβ specific binding proteins,[43,44] the chiral discrimination between these enantiomers was really attractive for targeting and inhibition of Aβ1−40 aggregation.

On the basis of the above results, we used different Aβ fragments, Aβ25−35 and Aβ12−28, to explore the metal complex binding site on Aβ1−40. Previous studies have shown that the Aβ25−35 fragment can, like Aβ1−40, form Aβ fibrils.[45−47] However, under our experimental conditions, both the inhibition and destabilization effects of these metal complexes on Aβ25−35 were much weaker (Figures S8B and S12, Supporting Information; Table 1); the two pairs of metal complexes did not inhibit the aggregation completely even at a very high concentration, indicating that these metal complexes bind weakly to Aβ25−35.

The form of the metallohelices studied here, with an overall 4+ charge, and three nonplanar hydrophobic ligands comprising an assembly of about 1.2 nm diameter, was proposed to be compatible with binding to the Aβ13−23 region. To confirm our hypothesis, a competitive binding assay using 4,4′-bis(1-anilinonaphthalene-8-sulfonate) (bis-ANS)[21,48] was employed. Bis-ANS recognizes soluble α-helical or random coil/mixed Aβ conformers at acidic pH; the fluorescence intensity is strongly enhanced upon binding. These metal complexes bound competitively with bis-ANS to Aβ1−40 as shown by fluorescence quenching data. Fitting with the Stern−Volmer equation yielded quenching constants of $2.29 \times 10^6$, $1.23 \times 10^6$, $1.29 \times 10^6$, and $6.11 \times 10^5$ $M^{-1}$ for **Λ1**, **Δ1**, **Λ2**, and **Δ2**, respectively (Figure S13A, Supporting Information). These results imply that the binding site for the metal complexes is similar to that of bis-ANS. For Aβ12−28, similar competitive binding results were obtained, and the quenching constants were $2.46 \times 10^6$, $1.37 \times 10^6$, $1.50 \times 10^6$, and $7.86 \times 10^5$ $M^{-1}$ for **Λ1**, **Δ1**, **Λ2**, and **Δ2**, respectively (Figure S13B). Therefore, these metal complexes may bind to the Aβ12−28 region, the central hydrophobic domain of Aβ1−40.

To further study the binding site, we carried out digestion experiments with trypsin.[16,21] Complex **2** was taken as an example. We chose Aβ12−28 as the trypsin substrate; the cleavage site (lysine residues) was just next to the central hydrophobic region. It was clearly shown that complex **2** could prevent the digestion of this fragment (Figure 3C), which indicated that complex **2** did bind to this hydrophobic region of the Aβ1−40 peptide. Therefore, our enzyme digestion experiments, inhibition data, circular dichroism, fluorescence quenching, and competitive binding results indicated that these metallosupramolecular complexes bound to the Aβ central region covering the α/β-discordant stretch of Aβ13−23, which had a helical size similar to that of the metal complexes.

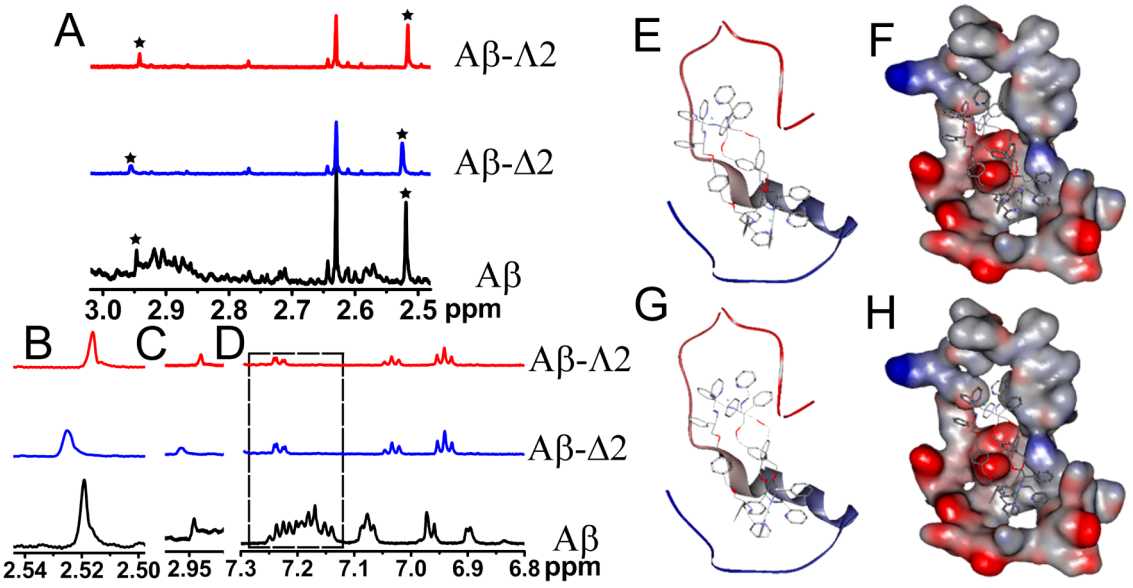


**Figure 4.** $^1$H NMR spectra of Aβ1−40 before and after treatment with the two enantiomers of complex **2**. (A) The signals of Aβ1−40 from amide protons of K16, F19, and E22 showed different shifts (see the peaks marked with asterisks). (B) Locally amplified $^1$H NMR spectra in (A) centered at 2.52 ppm. (C) Locally amplified $^1$H NMR spectra in (A) centered at 2.95 ppm. (D) The peaks due to the protons of F19 and F20 (see the box centered at 7.2 ppm) were significantly reduced in intensity after incubation with complex **2**. The signals of Aβ1−40 were assigned on the basis of literature values.[51−55] Energy-minimized average models of **Λ1** (E, F) and **Δ1** (G, H) with Aβ interactions. Cartoon (left) and surface (right) representations of complex **1** interacting with Aβ in the 13−23 region of the Aβ1−40 peptide.


dx.doi.org/10.1021/ja502789e | J. Am. Chem. Soc. 2014, 136, 11655−11663

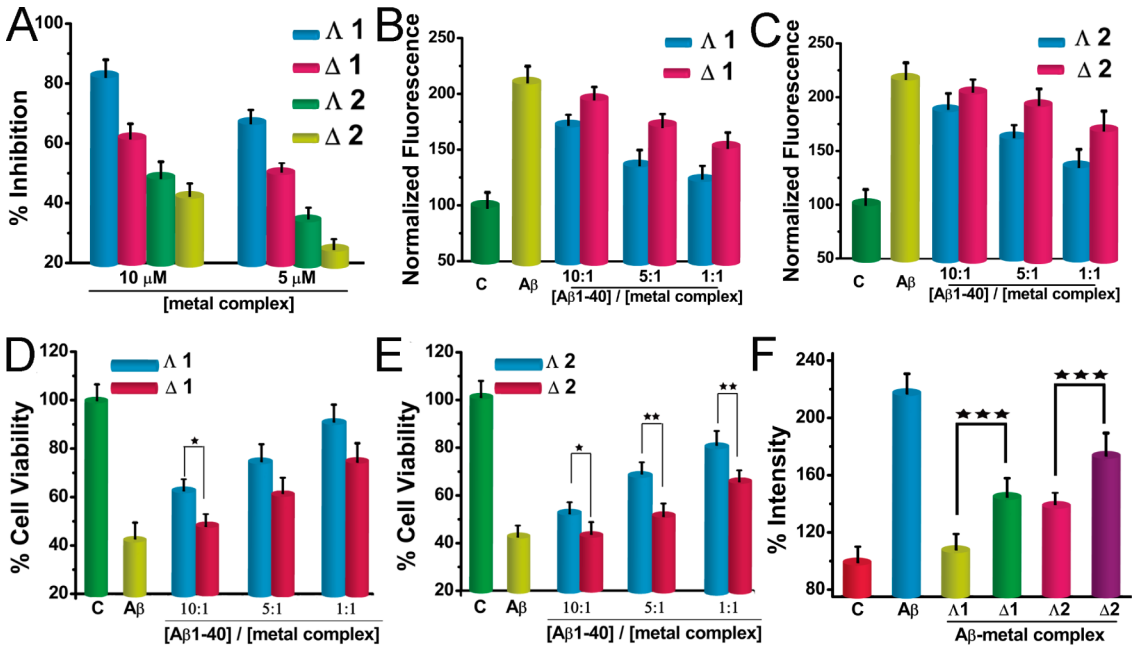


**Figure 5.** (A) Percent inhibition of NBT oxidation by superoxide radicals generated in the riboflavin−NBT−light system in vitro assessed by $NBT^+$ absorption at 560 nm with complexes **1** and **2**. (B, C) Effect of the metal complexes on ROS production in PC12 cells. Cells were treated with aged A$\beta$1−40 at a concentration of 5 $\mu$M in the absence or presence of increasing concentration of metal complexes, and 12 h later ROS generation inside the cells was measured using dichlorodihydrofluorescein (DCF) fluorescence. (D, E) Protection effects of metallosupramolecular complexes on A$\beta$1−40-induced cytotoxicity of PC 12 cells. The concentration of A$\beta$1−40 was 5 $\mu$M. (F) Inhibition of A$\beta$-induced calcium uptake by metal complexes. Cells were exposed to 5 $\mu$M A$\beta$1−40 or 5 $\mu$M A$\beta$1−40 pretreated with metal complexes at concentrations of 5 $\mu$M. After 2 h the cells were washed, fixed, and incubated in medium containing the cell-permeant calcium-sensitive dye Fluo-3 AM, as described in the Methods. The data points shown are the mean values ± standard error of the mean (SEM) from three independent experiments. Key: *, $P < 0.05$; **, $P < 0.01$; ***, $P < 0.001$. The control was A$\beta$-untreated cells.

The above results disclosed a remarkable stereoselective interaction between A$\beta$ and chiral metallosupramolecular complexes. The benzene rings at the center of the metal complex (Figure S1, Supporting Information) are stacked together by face−edge $\pi$ interactions and form a strong $\pi$ surface, and the aryl-lined cavities also have the potential to trap small molecules.[12−14] The aromatic amino acid residues in the central hydrophobic region of A$\beta$1−40, phenylalanines F19 and F20, can bind to the surface of the central benzene rings of the metal complex through hydrophobic interaction and $\pi-\pi$ stacking. As for A$\beta$1−40, $\pi-\pi$ stacking is also one of the most important factors influencing its physical and chemical behaviors.[49,50] Due to the $\alpha$-helical structure of the main chain and the chirality of L-amino acids that comprise the peptides, A$\beta$1−40 would exhibit different hydrophobic interactions and $\pi-\pi$ stacking with the $\Delta/\Lambda$ enantiomers. In addition, the positive charges of the two metal centers would not only increase the compounds' solubility but also enhance their binding ability to negatively charged A$\beta$ through electronic interactions.

The binding sites and different binding models between the chiral metal complexes and A$\beta$1−40 were further confirmed by NMR spectroscopy.[51−55] The $^1$H NMR signals of the aromatic moieties (F19F20)[51,52] of A$\beta$1−40 underwent remarkable changes upon addition of complex **2**, revealing their interactions associated with these units (Figure 4A,D). The metal complexes can bind to the hydrophobic core fragment of A$\beta$1−40, which was consistent with our above results. In addition, compared with the NMR spectrum of A$\beta$1−40 alone, there were obvious peak shifts in the signals from the amide protons of K16 (2.95 ppm) and E22 (2.52 ppm) in the presence of **Λ2** and **Δ2** (Figure 4B,C).[54,55] The NMR spectrum of A$\beta$1−40 in the presence of **Λ2** (Figure 4, blue) was different from that of A$\beta$1−40 treated with **Δ2**. **Λ2** caused the peaks to shift to the lower field, while **Δ2** made them move to the higher field, suggesting that **Λ2** and **Δ2** bound differently with A$\beta$1−40 in the 16−23 sequence.

Previous studies have shown that the L-amino acid residues usually arrange in a specific orientation on the surface of A$\beta$1−40, making A$\beta$1−40 sensitive to a chiral environment.[11,17] Since the chiral metal complex has a triple-helical array structure and is comparable in size to the A$\beta$1−40 peptide,[18] the large surface of the metal complex could stack on the peptide molecule. Considering the different effects of steric hindrance caused by the large pyridylimine unit and the helical chirality of the metallosupramolecular complex, the L-amino acid residues arranged on the surfaces of the A$\beta$1−40 peptide could exhibit different hydrophobic interactions with the $\Delta/\Lambda$ enantiomers, resulting in observed different peak shifts in the signals from the amide protons of K16 and E22 (Figure 4) and different enantioselectivities indicated by dialysis studies. Therefore, the enantioselective interactions between A$\beta$1−40 and chiral metallosupramolecular complexes might be due to the high stereospecific binding between these metal molecules and the local binding domain in the A$\beta$1−40 peptide.

To better understand and visualize the interactions of metal complexes with the monomeric A$\beta$1−40 peptide, docking studies were carried out on the basis of the previously reported NMR structure of monomeric A$\beta$1−40 (PDB 2LFM) in an aqueous environment using AutoDock Vina.[23,56,57] Although multiple structures of A$\beta$ (PDB 2LFM, 1IYT, 1BA4, 1ZE9, etc.)[56] have been reported, we employed the structure obtained


dx.doi.org/10.1021/ja502789e | J. Am. Chem. Soc. 2014, 136, 11655−11663

in an aqueous environment to carry out our study. Under this condition, the A$\beta$1−40 peptide contained a $3_{10}$ helix in the central hydrophobic region (residues 13−23) and collapsed in the N- and C-termini.[34] Furthermore, the helical intermediates in early fibrillogenesis events could convert into $\beta$ structures, which is in agreement with our experimental results. The structures of the A$\beta$1−40 and metal complexes used to perform the docking studies were shown in Figure S14 (Supporting Information). Figure 4 provided the low-energy conformations of A$\beta$1−40−metal complexes. Complex **1** was positioned in the 13−23 region of the A$\beta$1−40 peptide, further supporting that the metal complexes inhibited A$\beta$ aggregation by blocking the intermolecular interactions of multiple A$\beta$1−40 molecules. The two enantiomers of complex **2** binding to A$\beta$ were also shown in Figure S15 (Supporting Information). The binding energies of the four metal complexes with A$\beta$1−40 were summarized in Table S1 (Supporting Information). Although the accuracy of binding affinity predictions determined using Autodock Vina has improved substantially over that of previous Autodock iterations, errors of up to several kilocalories per mole remain possible.[58] Nevertheless, the predicted conformations reported here support our NMR data that the chiral metal complex bound to the hydrophobic region from K16 to E22.

It has been proposed that A$\beta$ can cause signaling amplification that inactivates SOD-2 and generates additional free radicals.[59] Moreover, AD model mice crossed with SOD-2 heterozygous knock out mice exhibited increased plaque deposition and tau phosphorylation in their brain.[60] Administration SOD reduces hippocampal superoxide and prevents memory deficits in a mouse model of AD.[61,62] Low molecular weight catalysts which mimic the SOD enzyme function, obtained by rational design and synthesis, are promising for use as a human pharmaceutical in the treatment of AD. It is known that certain metal-containing model compounds show catalase and/or SOD activity.[63,64] Reports have appeared on the SOD-like activity of the iron(III) derivative of porphyrin.[64] Considering these facts, we speculated that the iron supramolecular complex we used here may form an active artificial enzyme center and show SOD activity.

The SOD activities of these metal complexes were quantified using a modified NBT assay system.[65,66] The NBT assay was based on the capacities of these metal complexes to inhibit the reduction of NBT by photochemically generated superoxide anion radical in the presence of riboflavin. As shown in Figure 5A, due to the different absolute configurations at the metal, the complexes displayed different SOD mimic activities. The $\Lambda_{Fe}$ enantiomers were more effective than the $\Delta_{Fe}$ enantiomers.

Next we investigated the effects of the metal complexes on ROS production generated by A$\beta$1−40 aggregation in PC12 cells, which has been suggested as one proposed mechanism of AD pathogenesis. Our results indicated that the metal complexes could effectively suppress the A$\beta$1−40-induced ROS production (Figure 5B,C). On the basis of these data, these metal complexes could act as not only SOD mimics but also free radical scavengers.

The ability of these metal complexes to inhibit A$\beta$ assembly suggested that they might be useful in blocking A$\beta$-mediated cellular toxicity. To address this question, we used differentiated PC12 cells to perform MTT assay to probe cellular metabolism.[21,32−34] Cells, forced to undergo neuronal differentiation, have been demonstrated to mimic the neurons in the brain and be more sensitive to neurotoxicity of A$\beta$ aggregation than normal PC12 cells.[34] As shown in Figure 5D,E, aged A$\beta$1−40 led to a decrease of 42% in cellular reduction of MTT. Complex **1** or **2** could prevent cell death in a dose-dependent manner. Complex **1** or **2** alone, under our experimental conditions and concentration range, had little effect on PC 12 cell viability (Figure S16, Supporting Information), showing their low toxicity against PC12 cells. As expected, due to their different binding affinities to A$\beta$1−40, the $\Lambda_{Fe}$ enantiomers were more effective than the $\Delta_{Fe}$ enantiomers to inhibit A$\beta$-induced cytotoxicity, which demonstrated that the chiral discrimination of these metal complexes was obvious even in the complex culture medium. However, complex **1** showed a slightly stronger protection effect than complex **2**, indicating that A$\beta$-induced cytotoxicity was complicated when A$\beta$1−40 and the metal complexes were incubated together, although complex **1** had a higher binding affinity to A$\beta$1−40.

It has been proposed that one of the neurotoxic mechanisms of A$\beta$ is a direct consequence of the ability of A$\beta$ to form calcium channels in the target neurons. Perturbation of calcium homeostasis may also contribute to a self-amplifying cascade of free radical- and $Ca^{2+}$-mediated degenerative processes involved in the neurodegenerative phenotype of Alzheimer's disease.[67−69] Effective blocking of the A$\beta$-formed calcium channel can be critical for protection of the cells from A$\beta$ cytotoxicity. To test the hypothesis that these metal complexes interfere with the A$\beta$-dependent intracellular calcium change, we used the cell-permeant calcium-sensitive dye Fluo-3 AM to measure intracellular calcium levels in treated cells. As shown in Figure 5F, calcium accumulation in the A$\beta$-treated cells was substantial and statistically significant in the absence of the metal complexes. In contrast, in the presence of either complex **1** or complex **2**, a significant decrease of calcium accumulation was observed. Therefore, these metal complexes interfered with the A$\beta$-induced intracellular calcium change. Importantly, the enantioselectivity of these metal complexes was also obvious. The $\Lambda$ enantiomers could block the A$\beta$ calcium channel more effectively than the $\Delta_{Fe}$ enantiomers.

As suitable candidates for AD treatment, these metal complexes should cross the blood−brain barrier (BBB). To determine whether complexes **1** and **2** could passively accumulate in the brain of living animals, we used ICP-MS to measure the amount of Fe in the mouse brain after intraperitoneal injection for 4 h. A significant level of Fe was found in the cerebrospinal fluid (CSF) of the mouse treated with metal complexes compared to the control mouse. The efficiencies of Fe accumulation in the brain were 1.5% and 0.7% for complexes **1** and **2**, respectively, indicating these metal complexes possessed the ability to cross the BBB. These results further support that these metal complexes can act as promising therapeutic agents for AD treatment. Furthermore, compared with complex **1**, complex **2** showed a weaker ability to cross the BBB, which could be due to the larger size.

It is worth noting that these metal complexes with three-dimensional (3D) structures were comparable in size to the A$\beta$1−40 peptide. Strong attraction between the peptide molecules and metal complexes would result in their stacking around the edges of the metal complexes and concomitant scrambling of the 3D lock-and-key match between the neighboring peptide molecules.[70] A similar mechanism was observed for inorganic nanoparticles but without the chiral effects.[70] This would further inhibit the self-assembly of A$\beta$1−40 and affect the physiological functions of the A$\beta$ species. As shown in our results from the ThT assay, CD, and AFM, the metal complexes can effectively inhibit A$\beta$1−40 aggregation

and cross the BBB. In addition, the A$\beta$-formed calcium channel, A$\beta$-mediated cellular toxicity, and ROS production can also be blocked by the metal complexes (Figure 5). Polyvalency is a powerful means for designing ligands that bind more strongly to targets.[71,72] Metallosupramolecular assembly can combine the concept for design of small inhibitors and further amplify the role of stereochemistry due to the multivalency and selectable size and configuration of the ligand. This may provide new insights into chiral inhibition of A$\beta$ aggregation.

## CONCLUSION

In summary, two triple-helical dinuclear metallosupramolecular complexes have been identified as a novel class of chiral amyloid-$\beta$ inhibitors. Through targeting $\alpha/\beta$-discordant stretches at the early steps of aggregation, these chiral metal complexes can enantioselectively inhibit A$\beta$ aggregation, which is demonstrated using fluorescent cell-based screening and multiple biophysical and biochemical approaches. To the best of our knowledge, there are no reports of enantioselective targeting and inhibition of A$\beta$ aggregation. Chiral discrimination is an important subject for AD treatment. Our work may open a new avenue for design and screening of chiral supramolecular complexes as A$\beta$ inhibitors against AD.

## ASSOCIATED CONTENT

### Supporting Information

Experimental details and characterization data. This material is available free of charge via the Internet at http://pubs.acs.org.

## AUTHOR INFORMATION

### Corresponding Author

xqu@ciac.ac.cn

### Notes

The authors declare no competing financial interest.

## ACKNOWLEDGMENTS

This work was supported by the 973 Project (Grants 2011CB936004 and 2012CB720602) and National Natural Science Foundation of China (NSFC) (Grants 21210002, 21431007, and 91213302).

## REFERENCES

(1) Blennow, K.; de Leon, M. J.; Zetterberg, H. *Lancet* **2006**, *368*, 387−403.
(2) Rauk, A. *Chem. Soc. Rev.* **2009**, *38*, 2698−2715.
(3) Jakob-Roetne, R.; Jacobsen, H. *Angew. Chem., Int. Ed.* **2009**, *48*, 3030−3059.
(4) Gaggelli, E.; Kozlowski, H.; Valensin, D.; Valensin, G. *Chem. Rev.* **2006**, *106*, 1995−2044.
(5) Hamley, I. W. *Chem. Rev.* **2012**, *112*, 5147−5192.
(6) Cassagnes, L. E.; Hervé, V.; Nepveu, F.; Hureau, C.; Faller, P.; Collin, F. *Angew. Chem., Int. Ed.* **2013**, *52*, 11110−11113.
(7) Pedersen, J. T.; Hureau, C.; Hemmingsen, L.; Heegaard, N. H. H.; Ostergaard, J.; Vasak, M.; Faller, P. *Biochemistry* **2012**, *51*, 1697−1706.
(8) Yang, F.; Lim, G. P.; Begum, A. N.; Ubeda, O. J.; Simmons, M. R.; Ambegaokar, S. S.; Chen, P.; Kayed, R.; Glabe, C. G.; Frautschy, S. A.; Cole, G. M. *J. Biol. Chem.* **2005**, *280*, 5892−5901.
(9) Barnham, K. J.; Kenche, V. B.; Ciccotosto, G. D.; Smith, D. P.; Tew, D. J.; Liu, X.; Perez, K.; Cranston, G. A.; Johanssen, T. J.; Volitakis, I.; Bush, A. I.; Masters, C. L.; White, A. R.; Smith, J. P.; Cherny, R. A.; Cappai, R. *Proc. Natl. Acad. Sci. U.S.A.* **2008**, *105*, 6813−6818.
(10) Ehrnhoefer, D. E.; Bieschke, J.; Boeddrich, A.; Herbst, M.; Masino, L.; Lurz, R.; Engemann, S.; Pastore, A.; Wanker, E. E. *Nat. Struct. Mol. Biol.* **2008**, *15*, 558−566.
(11) Sood, A.; Abid, M.; Hailemichael, S.; Foster, M.; Török, B.; Török, M. *Bioorg. Med. Chem. Lett.* **2009**, *19*, 6931−6934.
(12) Nakanishi, T.; Yamakawa, N.; Asahi, T.; Shibata, N.; Ohtani, B.; Osaka, T. *Chirality* **2004**, *16*, S36−S39.
(13) Schapira, A. H. V.; Emre, M.; Jenner, P.; Poewe, W. *Eur. J. Neurol.* **2009**, *16*, 982−989.
(14) Kallberg, Y.; Gustafsson, M.; Persson, B.; Thyberg, J.; Johansson, J. *J. Biol. Chem.* **2001**, *276*, 12945−12950.
(15) Nerelius, C.; Sandegren, A.; Sargsyan, H.; Raunak, R.; Leijonmarck, H.; Chatterjee, U.; Fisahn, A.; Imarisio, S.; Lomas, D. A.; Crowther, D. C.; Stromberg, R.; Johansson, J. *Proc. Natl. Acad. Sci. U.S.A.* **2009**, *106*, 9191−9196.
(16) Yu, H.; Li, M.; Liu, G.; Geng, J.; Wang, J.; Ren, J.; Zhao, C.; Qu, X. *Chem. Sci.* **2012**, *3*, 3145−3153.
(17) Rubin, N.; Perugia, E.; Goldschmidt, M.; Fridkin, M.; Addadi, L. *J. Am. Chem. Soc.* **2008**, *130*, 4602−4603.
(18) Howson, S. E.; Bolhuis, A.; Brabec, V.; Clarkson, G. J.; Malina, J.; Rodger, A.; Scott, P. *Nat. Chem.* **2012**, *4*, 31−36.
(19) Hannon, M. J.; Meistermann, I.; Isaac, C. J.; Blomme, C.; Aldrich-Wright, J. R.; Rodger, A. *Chem. Commun.* **2001**, 1078−1079.
(20) Brabec, V.; Howson, S. E.; Kaner, R. A.; Lord, R. M.; Malina, J.; Phillips, R. M.; Abdallah, Q. M. A.; McGowan, P. C.; Rodger, A.; Scott, P. *Chem. Sci.* **2013**, *4*, 4407−4416.
(21) Geng, J.; Li, M.; Ren, J.; Wang, E.; Qu, X. *Angew. Chem., Int. Ed.* **2011**, *50*, 4184 −4188.
(22) Kim, W.; Kim, Y.; Min, J.; Kim, D. J.; Chang, Y.-T.; Hecht, M. H. *ACS Chem. Biol.* **2006**, *1*, 461−469.
(23) Gao, N.; Sun, H.; Dong, K.; Ren, J.; Duan, T.; Xu, C.; Qu, X. *Nat. Commun.* **2014**, *5*, 3422.
(24) Levine, H. *Protein Sci.* **1993**, *2*, 404−410.
(25) Yang, W.; Wong, Y.; Ng, O. T. W.; Bai, L.-P.; Kwong, D. W. J.; Ke, Y.; Jiang, Z.-H.; Li, H.-W.; Yung, K. K. L.; Wong, M. S. *Angew. Chem., Int. Ed.* **2012**, *51*, 1804 −1810.
(26) Cabaleiro-Lago, C.; Quinlan-Pluck, F.; Lynch, I.; Lindman, S.; Minogue, A. M.; Thulin, E.; Walsh, D. M.; Dawson, K. A.; Linse, S. *J. Am. Chem. Soc.* **2008**, *130*, 15437−15443.
(27) Mishra, R.; Bulic, B.; Sellin, D.; Jha, S.; Waldmann, H.; Winter, R. *Angew. Chem., Int. Ed.* **2008**, *47*, 4679−4682.
(28) Sandberg, A.; Luheshi, L. M.; Söllvander, S.; de Barros, T. P.; Macao, B.; Knowles, T. P. J.; Biverstål, H.; Lendel, C.; Ekholm-Petterson, F.; Dubnovitsky, A.; Lannfelt, L.; Dobson, C. M.; Härd, T. *Proc. Natl. Acad. Sci. U.S.A.* **2010**, *107*, 15595−15600.
(29) Sakono, M.; Zako, T. *FEBS J.* **2010**, *277*, 1348−1358.
(30) Olesen, O. F.; Dagø, L. *Biochem. Biophys. Res. Commun.* **2000**, *270*, 62−66.
(31) Bieschke, J.; Herbst, M.; Wiglenda, T.; Friedrich, R. P.; Boeddrich, A.; Schiele, F.; Kleckers, D.; del Aamo, J. M. L.; Grüning, B. A.; Wang, Q.; Schmidt, M. R.; Lurz, R.; Anwy, R.; Schnoeg, S.; Fändrich, M.; Frank, R. F.; Rreif, B.; Günther, S.; Walsh, D. M.; Wanker, E. E. *Nat. Chem. Biol.* **2012**, *8*, 93−101.
(32) Bieschke, J.; Russ, J.; Friedrich, R. P.; Ehrnhoefer, D. E.; Wobst, H.; Neugebauer, K.; Wanker, E. E. *Proc. Natl. Acad. Sci. U.S.A.* **2010**, *107*, 7710−7715.
(33) Li, M.; Yang, X.; Ren, J.; Qu, K.; Qu, X. *Adv. Mater.* **2012**, *24*, 1722−1728.
(34) Li, M.; Shi, P.; Xu, C.; Ren, J.; Qu, X. *Chem. Sci.* **2013**, *4*, 2536−2542.
(35) Qu, X.; Trent, J. O.; Fokt, I.; Priebe, W.; Chaires, J. B. *Proc. Natl. Acad. Sci. U.S.A.* **2000**, *97*, 12032−12037.
(36) Song, G.; Xing, F.; Qu, X.; Chaires, J. B.; Ren, J. *J. Med. Chem.* **2005**, *48*, 3471−3473.
(37) Man, B. Y.-W.; Chan, H.-M.; Leung, C.-H.; Chan, D. S.-H.; Bai, L.-P.; Jiang, Z.-H.; Li, H.-W.; Ma, D.-L. *Chem. Sci.* **2011**, *2*, 917−921.
(38) Sinha, S.; Lopes, D. H. J.; Du, Z.; Pang, E. S.; Shanmugam, A.; Lomakin, A.; Talbiersky, P.; Tennstaedt, A.; McDaniel, K.; Bakshi, R.; Kuo, P.-Y.; Ehrmann, M.; Benedek, G. B.; Loo, J. A.; Klärner, F.-G.;

Schrader, T.; Wang, C.; Bitan, G. *J. Am. Chem. Soc.* **2011**, *133*, 16958−16969.
(39) Yu, H.; Ren, J.; Qu, X. *Biophys. J.* **2007**, *92*, 185−191.
(40) Yu, H.; Ren, J.; Qu, X. *ChemBioChem* **2008**, *9*, 879−882.
(41) Schlamadinger, D. E.; Kats, D. I.; Kim, J. E. *J. Chem. Educ.* **2010**, *87*, 961−964.
(42) Puchalski, M. M.; Morra, M. J.; von Wandruszka, R. *Fresenius' J. Anal. Chem.* **1991**, *340*, 341−344.
(43) Costa, R.; Gonçalves, A.; Saraiva, M. J.; Cardoso, I. *FEBS Lett.* **2008**, *582*, 936−942.
(44) Deane, R.; Wu, Z.; Sagare, A.; Davis, J.; Yan, S.; Hamm, K.; Xu, F.; Parisi, M.; LaRue, B.; Hu, H.; Spijkers, P.; Guo, H.; Song, X.; Lenting, P. J.; Van Nostrand, W. E.; Zlokovic, B. V. *Neuron* **2004**, *43*, 333−344.
(45) Zhang, H.; Liang, Y.; Tang, X.; He, X.; Bai, D. *Neurosci. Lett.* **2002**, *317*, 143−146.
(46) Kanekiyo, T.; Ban, T.; Aritake, K.; Huang, Z.; Qu, W.; Okazaki, I.; Mohri, I.; Murayama, S.; Ozono, K.; Taniike, M.; Goto, Y.; Urade, Y. *Proc. Natl. Acad. Sci. U.S.A.* **2007**, *104*, 6412−6417.
(47) Fu, Z.; Luo, Y.; Derreumaux, P.; Wei, G. *Biophys. J.* **2009**, *97*, 1795−1803.
(48) LeVine, H., III. *Arch. Biochem. Biophys.* **2002**, *404*, 106−115.
(49) Yan, X.; Zhu, P.; Fei, J.; Li, J. *Adv. Mater.* **2010**, *22*, 1283−1287.
(50) Ikeda, M.; Tanida, T.; Yoshii, T.; Hamachi, I. *Adv. Mater.* **2011**, *23*, 2819−2822.
(51) Ma, G.; Huang, F.; Pu, X.; Jia, L.; Jiang, T.; Li, L.; Liu, Y. *Chem.—Eur. J.* **2011**, *17*, 11657−11666.
(52) Zhang, X.; Tian, Y.; Li, Z.; Tian, X.; Sun, H.; Liu, H.; Moore, A.; Ran, C. *J. Am. Chem. Soc.* **2013**, *135*, 16397−16409.
(53) Hamley, I. W.; Nutt, D. R.; Brown, G. D.; Miravet, J. F.; Escuder, B.; Rodríguez-Llansola, F. *J. Phys. Chem. B* **2010**, *114*, 940−951.
(54) Scherzer-Attali, R.; Pellarin, R.; Convertino, M.; Frydman-Marom, A.; Egoz-Matia, N.; Peled, S.; Levy-Sakin, M.; Shalev, D. E.; Caflisch, A.; Gazit, E.; Segal, D. *PLoS One* **2010**, *5*, e11101−e11115.
(55) Zagorski, M. G.; Barrow, C. J. *Biochemistry* **1992**, *31*, 5621−5631.
(56) Vivekanandan, S.; Brender, J. R.; Lee, S. Y.; Ramamoorthy, A. *Biochem. Biophys. Res. Commun.* **2011**, *411*, 312−316.
(57) Trott, O.; Olson, A. J. *J. Comput. Chem.* **2010**, *31*, 455−461.
(58) Veloso, A. J.; Chow, A. M.; Ganesh, H. V. S.; Li, N.; Dhar, D.; Wu, D. C. H.; Mikhaylichenko, S.; Brown, I. R.; Kerman, K. *Anal. Chem.* **2014**, *86*, 4901−4909.
(59) Massaad, C. A.; Washington, T. M.; Pautler, R. G.; Klann, E. *Proc. Natl. Acad. Sci. U.S.A.* **2009**, *106*, 13576−13581.
(60) Li, F.; Calingasan, N. Y.; Yu, F.; Mauck, W. M.; Toidze, M.; Almeida, C. G.; Takahashi, R. H.; Carlson, G. A.; Beal, M. F.; Lin, M. T.; Gouras, G. K. *J. Neurochem.* **2004**, *89*, 1308−1312.
(61) Riley, D. P. *Chem. Rev.* **1999**, *99*, 2573−2587.
(62) Sompol, P.; Ittarat, W.; Tangpong, J.; Chen, Y.; Doubinskaia, I.; Batinic-Haberle, I.; Abdul, H. M.; Butterfield, D. A.; Clair, D. K. St. *Neuroscience* **2008**, *153*, 120−130.
(63) Doctrow, S. R.; Huffman, K.; Marcus, C. B.; Tocco, G.; Malfroy, E.; Adinolfi, C. A.; Kruk, H.; Baker, K.; Lazarowych, N.; Mascarenhas, J.; Malfroy, B. *J. Med. Chem.* **2002**, *45*, 4549−4558.
(64) Pasternack, R. F.; Halliwell, B. *J. Am. Chem. Soc.* **1979**, *101*, 1026−1031.
(65) Geng, J.; Li, M.; Wu, L.; Ren, J.; Qu, X. *J. Med. Chem.* **2012**, *55*, 9146−9155.
(66) Wu, Y.; Wang, D. *J. Proteome Res.* **2009**, *8*, 436−442.
(67) Arispe, N.; Pollard, H. B.; Rojas, E. *Proc. Natl. Acad. Sci. U.S.A.* **1996**, *93*, 1710−1715.
(68) Arispe, N.; Rojas, E.; Pollard, H. B. *Proc. Natl. Acad. Sci. U.S.A.* **1993**, *90*, 567−571.
(69) Diaz, J. C.; Simakova, O.; Jacobson, K. A.; Arispe, N.; Pollard, H. B. *Proc. Natl. Acad. Sci. U.S.A.* **2009**, *106*, 3348−3353.
(70) Yoo, S. I.; Yang, M.; Brender, J. R.; Subramanian, V.; Sun, K.; Joo, N. E.; Jeong, S.-H.; Ramamoorthy, A.; Kotov, N. A. *Angew. Chem., Int. Ed.* **2011**, *50*, 5110−5115.
(71) Mourtas, S.; Canovi, M.; Zona, C.; Aurilia, D.; Niarakis, A.; La Ferla, B.; Salmona, M.; Nicotra, F.; Gobbi, M.; Antimisiaris, S. G. *Biomaterials* **2011**, *32*, 1635−1645.
(72) Cheng, P.-N.; Spencer, R.; Woods, R. J.; Glabe, C. G.; Nowick, J. S. *J. Am. Chem. Soc.* **2012**, *134*, 14179−14184.